Hindawi
Advances in Mathematical Physics
Volume 2024, Article ID 7253630, 10 pages
https://doi.org/10.1155/2024/7253630

Research Article

Aspects of Non-unique Solutions for Hiemenz Flow Filled with Ternary Hybrid Nanofluid over a Stretching/Shrinking Sheet

Farah Nadzirah Jamrus,[1,2] **Anuar Ishak**,[2] **Iskandar Waini**,[3] **Umair Khan**,[2,4] **Md Irfanul Haque Siddiqui**,[5] **and J. K. Madhukesh**[6]

[1]*Kolej Pengajian Pengkomputeran, Informatik dan Matematik, Universiti Teknologi MARA (UiTM), Cwgn Melaka Kampus Jasin, Merlimau, Melaka 77300, Malaysia*
[2]*Department of Mathematical Sciences, Faculty of Science and Technology, Universiti Kebangsaan Malaysia, UKM, Bangi 43600, Selangor, Malaysia*
[3]*Fakulti Teknologi dan Kejuruteraan Industri dan Pembuatan, Universiti Teknikal Malaysia Melaka, Hang Tuah Jaya, Durian Tunggal, Melaka 76100, Malaysia*
[4]*Department of Computer Science and Mathematics, Lebanese American University, Byblos, Lebanon*
[5]*Mechanical Engineering Department, College of Engineering, King Saud University, Riyadh 11451, Saudi Arabia*
[6]*Department of Mathematics, Amrita School of Engineering, Amrita Vishwa Vidyapeetham, Bengaluru, India*

Correspondence should be addressed to Umair Khan; umair.khan@lau.edu.lb

Received 24 October 2023; Revised 14 December 2023; Accepted 22 December 2023; Published 10 January 2024

Academic Editor: Ghulam Rasool

This study is carried out to scrutinize the Hiemenz flow for ternary hybrid nanofluid flow across a stretching/shrinking sheet. This study aims to inspect the impacts of variations in the stretching/shrinking parameter and the volume fraction of nanoparticles on key aspects of the ternary hybrid nanofluid flow, specifically the skin friction, Nusselt number (which relates to heat transfer), velocity profiles, and the temperature profiles. The flow equations transform into a system of ordinary differential equations (ODEs) using a similarity transformation. Subsequently, the system is numerically solved using the MATLAB software's 4th-order accuracy boundary value problem solver, known as "bvp4c". Numeric findings reveal that skin friction values exhibit variations based on the magnitude of the stretching/shrinking parameter. Moreover, in the specific context of the flow problem being studied, the heat conduction efficiency of the hybrid (ternary) nanofluid surpasses that of the hybrid nanofluid. The system yields two distinct solutions within a specific shrinking/stretching parameter interval. Through an examination of the temporal stability of the solutions, it was determined that only one remained stable over an extended period. Remember that these current findings hold solely for the combination of copper, alumina, and titania.

1. Introduction

Recently, researchers in fluid dynamics have emphasized exploring the properties of stagnation point flow. The fluid flow around the region positioned at the front end of a blunt-nosed object is commonly referred to as stagnation point flow. The phenomena mentioned above can be observed on any solid entity that is submerged in a fluid medium. In the stagnation region, the highest pressure results from force buildup due to halted flow, accompanied by rapid heat transfer and significant accumulation of particles or substances from the fluid, making it a critical location. The researchers have been attracted by the varied array of applications of stagnation point flow, including the process of extrusion, the polymer industry, and concerns linked to aerodynamics [1, 2]. The investigation of stagnation point flow is also crucial to understand physiological fluid dynamics, such as the way blood clots form artificial organs [3, 4]. The phenomenon of stagnation point flow over a stretching/shrinking sheet is commonly observed in the real-world application of the plastic extrusion. Extrusion is a manufacturing method that uses pressure to propel a material through a die, forming a consistent and uninterrupted profile. Throughout this procedure, the fluid dynamics experts utilize the velocity and temperature profile,

skin friction, and heat transfer rate to guarantee the final products' quality. Hiemenz [5] was among the pioneering researchers investigating stagnation point flow, and later, the problem was extended to the axisymmetric flow case [6]. Then, Mahapatra and Gupta [7] discovered the impact of heat transmission on the stagnation point flow past a plate that is stretched radially. Afterward, Wang [8] extended the idea to the axisymmetric stagnation point flow over a shrinking sheet, and the author's research highlights under the case of shrinking sheet, dual solutions occur in a particular shrinking parameter range. Following that, numerous captivating studies were conducted exploring the Hiemenz flow under the same boundary conditions, comprising a variety of physical parameters [9–12].

Water, ethylene glycol, ethanol, and glycerin play a crucial role in heating and cooling, power generation, and chemical processes. Nevertheless, as mentioned earlier, the heat transfer process is hindered due to the limited heat transfer of conventional fluids. Therefore, a new fluid type referred to as nanofluid was created by Choi and Eastman [13] to overcome the limitations of conventional fluids. Nanofluids consist of a kind of nanoparticle ranging in size from 1 to 100 nm that are dispersed in the base fluid. They have demonstrated that using nanofluids can improve thermal properties and enhance heat transport rates. Additionally, several relevant sources discussing the application of nanofluids to enhance heat transfer can be found in the investigations conducted by Mehobbiand Rashidi [14–16]. Later, researchers shifted their attention toward hybrid nanofluids, which are mixtures of nanoparticles from two distinct categories with the base fluid. These extended nanofluids demonstrated commendable heat conductivity characteristics and can boost the heat transfer rate in comparison to single nanofluids [12, 17–20].

The need for enhanced thermal conductivity and heat transmission has driven the development of ternary hybrid nanofluids, known as stable mixtures of three distinct varieties of nanoparticles in a base fluid, offering enhanced properties compared to single and hybrid nanofluids. This new extended nanofluid can help optimize heat transmission in various engineering and industrial settings [21]. Ramadhan et al. [22] dispersed Al_2O_3 (alumina), TiO_2 (titania), and SiO_2 (silica) in ethylene glycol to create a ternary hybrid nanofluid. In their experimental work, the authors found that ternary hybrid nanofluid possessed the best effective thermal conductivity when the concentration volume was 0.3% compared to 0.05%−0.2%. At the same time, Sundar et al. [23] suspended GO (graphene oxide), Fe3O4 (iron oxide), and TiO_2 nanoparticles in ethylene glycol to make ternary hybrid nanofluid. Their findings indicated that the system thermal efficacy of ternary hybrid nanofluids has increased to 14.32%. Besides, Animasaun et al. [24] evaluated the stagnation point flow concerning a stretching sheet involving ternary hybrid nanofluid Ag–Al_2O_3–Al/water (argentum–alumina–aluminium/water). The results revealed that increasing the Biot number between 0.1 and 3.0 increases the heat transfer rate of ternary hybrid nanofluids in situations involving heat generation/absorption. Gupta and Rana [25] examined the 3-D stagnation point flow of Ag–Al_2O_3_Al/water over a rotating and stretching disk. The research concluded that the ternary hybrid nanofluid possesses an enhanced heat conductivity compared to water, leading to an increased heat transfer rate.

The excellent thermophysical characteristics and rheological behavior of the Al_2O_3–Cu–TiO_2/water (alumina–copper–titania/water) ternary nanofluid were observed in an experiment done by Xuan et al. [26]. According to the authors in [25], when large Cu nanoparticles are present in a fluid, there is a notable physical separation or distance between these particles and the surrounding water molecules. This gap contributes to a high level of thermal contact resistance, which can hinder efficient heat transfer. When smaller sized Al_2O_3 and TiO_2 nanoparticles are introduced into the fluid, they fill in the gaps between the larger Cu nanoparticles. This action reduces the interparticle space and, as a result, improves the fluid's thermal properties.

As far as the authors know, no reported studies discuss stagnation point flow utilizing Al_2O_3–$CuTiO_2$/water as a ternary hybrid nanofluid. Hence, drawing inspiration from [25], we analyzed the heat transfer characteristics of the ternary hybrid nanofluid (Al_2O_3–Cu–TiO_2/water) in the context of stagnation point flow over a stretching/shrinking sheet. Additionally, this study may offer insights to engineers and researchers on strategies to increase or decrease heat transfer rates by controlling the parameters' values. Besides, the authors are concerned that this flow problem will produce more than one solution; hence, a stability analysis is conducted to determine the long-run stability of the solutions. Skin friction and Nusselt number comparison analyses are also conducted between ternary hybrid nanofluid and hybrid nanofluid.

2. Problem Formulation

This research focuses on examining the Hiemenz flow of a ternary hybrid Al_2O_3–Cu–TiO_2/water nanofluid over a stretching/shrinking sheet. Here, the flow overview is demonstrated in Figure 1.

The free stream and surface velocities are taken as $u_e(x) = ax$, and $u_w(x) = bx$, respectively, with a and b are considered as constants. The ambient temperature T_∞ and the wall temperature T_w also considered as constant.

Mathematically, the equations govern the flow problem are as follows [27]:

$$\frac{\partial u}{\partial x} + \frac{\partial v}{\partial y} = 0, \tag{1}$$

$$u\frac{\partial u}{\partial x} + v\frac{\partial u}{\partial y} = u_e\frac{du_e}{dx} + \frac{\mu_{thnf}}{\rho_{thnf}}\frac{\partial^2 u}{\partial y^2}, \tag{2}$$

$$u\frac{\partial T}{\partial x} + v\frac{\partial T}{\partial y} = \frac{k_{thnf}}{(\rho C_p)_{thnf}}\frac{\partial^2 T}{\partial y^2}, \tag{3}$$

subject to

$$\begin{aligned} &u = u_w(x), v = 0, T = T_w \text{ at } y = 0 \\ &u \to u_e(x), T \to T_\infty \text{ as } y \to \infty. \end{aligned} \tag{4}$$

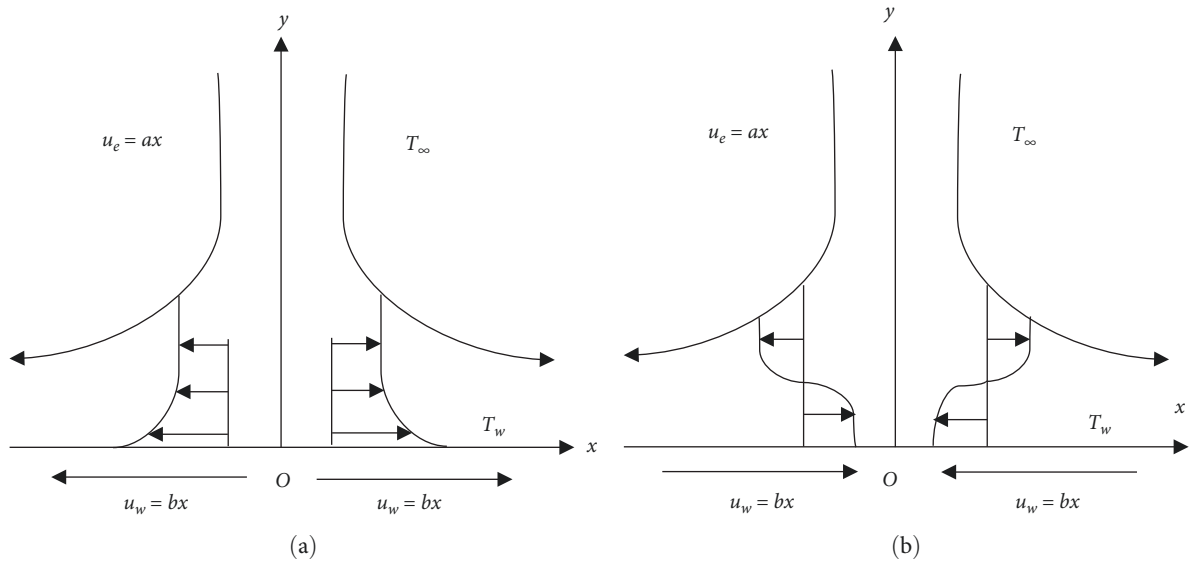

FIGURE 1: Flow overview: (a) stretching sheet and (b) shrinking sheet.

TABLE 1: Thermophysical properties with respect to ternary hybrid nanofluid as well as hybrid nanofluid [28, 29].

Property	Hybrid nanofluid	Ternary hybrid nanofluid
Dynamic viscosity	$\mu_{hnf} = \frac{\mu_{nf}}{(1-\varphi_1)^{2.5}(1-\varphi_2)^{2.5}}$	$\mu_{thnf} = \frac{\mu_{nf}}{(1-\varphi_1)^{2.5}(1-\varphi_2)^{2.5}(1-\varphi_3)^{2.5}}$
Density	$\rho_{hnf} = (1-\phi_2)[(1-\phi_1)\rho_f + \phi_1\rho_{n1}] + \phi_2\rho_{n2}$	$\rho_{thnf} = (1-\phi_3)\{(1-\phi_2)[(1-\phi_1)\rho_f + \phi_1\rho_{n1}] + \phi_2\rho_{n2}\} + \phi_3\rho_{n3}$
Heat capacity	$(\rho C_p)_{hnf} = (1-\phi_2)[(1-\phi_1)(\rho C_p)_f + \phi_1(\rho C_p)_{n1}] + \phi_2(\rho C_p)_{n2}$	$(\rho C_p)h_{thnf} = (1-\phi_3)\{(1-\phi_2)[(1-\phi_1)(\rho C_p)_f + \phi_1(\rho C_p)_{n1}] + \phi_2(\rho C_p)_{n2}\} + \phi_3(\rho C_p)_{n3}$
Thermal conductivity	$k_{hnf} = \frac{k_{n2} + 2k_{nf} - 2\phi_2(k_{nf} - k_{n2})}{k_{n2} + 2k_{nf} + \phi_2(k_{nf} - k_{n2})} \times (k_{nf})$ where $k_{nf} = \frac{k_{n1} + 2k_f - 2\phi_1(k_f - k_{n1})}{k_{n1} + 2k_f + \phi_1(k_f - k_{n1})} \times (k_f)$	$k_{thnf} = \frac{k_{n3} + 2k_{hnf} - 2\phi_3(k_{hnf} - k_{n3})}{k_{n3} + 2k_{hnf} + \phi_3(k_{hnf} - k_{n3})}$ where $k_{nf} = \frac{k_{n1} + 2k_f - 2\phi_1(k_f - k_{n1})}{k_{n1} + 2k_f + \phi_1(k_f - k_{n1})} \times (k_f)$ where $k_{hnf} = \frac{k_{n2} + 2k_{nf} - 2\phi_2(k_{nf} - k_{n2})}{k_{n2} + 2k_{nf} + \phi_2(k_{nf} - k_{n2})} \times (k_{nf})$

Here, (u, v) resembles the velocity component along the (x, y)-axis while T refers to the temperature. Meanwhile, the thermophysical properties with respect to hybrid nanofluid and ternary hybrid nanofluid are displayed in Tables 1 and 2 indicates the thermophysical properties of nanoparticles as well as water. The thermal conductivity, dynamic viscosity, density, as well as the heat capacity is symbolized as k, μ, ρ, and (ρC_p), respectively. It is essential to mention that subscripts nf, f, hnf as well as $thnf$ resembles the nanofluid, base fluid, hybrid nanofluid and ternary hybrid nanofluid, accordingly. Moreover, Al_2O_3 (subscript $n1$), Cu (subscript $n2$), and TiO_2 (subscripts $n3$) are the nanoparticles used in this research work and their volume fractions are depicted by φ_1, φ_2 as well as φ_3, accordingly.

Then, a set of dimensionless variables are introduced as follows [30]:

$$\psi = (a\nu_f)^{1/2}, \theta(\eta) = \frac{T - T_\infty}{T_w - T_\infty}, \eta = \left(\frac{a}{\nu_f}\right)^{1/2} y, \tag{5}$$

with ν_f denotes the base fluid kinematic viscosity, while ψ represents the stream function. By defining $u = \partial\psi/\partial y$ and $v = -\partial\psi/\partial x$ yields:

Table 2: Thermophysical properties with respect to nanoparticles and water [29].

Property	Al_2O_3	Cu	TiO_2	Water
$C_p(Jkg^{-1}K^{-1})$	765	385	686.5	4,179
$\rho(kgm^{-3})$	3,970	8,933	4,250	997.1
$k(Wm^{-1}K^{-1})$	40	400	8.9538	0.613
Prandtl number				6.2

$$u = axf'(\eta), v = -(a\nu_f)^{1/2} f(\eta). \tag{6}$$

By utilizing similarity variables in Equations (5) and (6), Equations (1)–(3) reduce and are expressed in the following form:

$$\frac{\mu_{thnf}/\mu_f}{\rho_{thnf}/\rho_f} f''' + ff'' + 1 - f'^2 = 0, \tag{7}$$

$$\frac{1}{Pr} \frac{k_{thnf}/k_f}{(\rho C_p)_{thnf}/(\rho C_p)_f} \theta'' + f\theta' = 0. \tag{8}$$

Subsequently, the initial and boundary conditions in Equation (4) experience a transformation in yielding the expressions given below:

$$\begin{aligned} &f(0) = 0, f'(0) = \lambda, \theta(0) = 1 \text{ at } \eta = 0, \\ &f'(\eta) \to 1, \theta(\eta) \to 0 \text{ as } \eta \to \infty, \end{aligned} \tag{9}$$

in which $\lambda = \frac{b}{a}$ refers to the parameter of shrinking/stretching. The negative values of λ represent the case of shrinking, while the stretching case is represented by λ possesses positive values, and $\lambda = 0$ specifies the nonmoving surface.

Meanwhile, Pr in Equation (8) is the Prandtl number that is defined as follows:

$$Pr = \frac{(\mu C_p)_f}{k_f}. \tag{10}$$

The coefficient of skin friction C_f and the local Nusselt number Nu_x resemble the crucial physical quantities in consideration which are defined as follows [27]:

$$C_f = \frac{\mu_{thnf}}{\rho_f u_e^2} \left(\frac{\partial u}{\partial y}\right)_{y=0}, Nu_x = \frac{xk_{thnf}}{k_f(T_w - T_\infty)} \left(\frac{\partial T}{\partial y}\right)_{y=0}. \tag{11}$$

The shear stress τ_w as well as the heat flux q_w at the surface are expressed as follows:

$$\tau_w = \mu_{thnf} \left(\frac{\partial u}{\partial y}\right)_{y=0}, q_w = -k_{thnf} \left(\frac{\partial T}{\partial y}\right)_{y=0}. \tag{12}$$

By implementing Equations (5) and (12) into Equation (11), gives:

$$Re_x^{1/2} C_f = \frac{\mu_{thnf}}{\mu_f} f''(0), Re_x^{-1/2} Nu_x = -\frac{k_{thnf}}{k_f} \theta'(0), \tag{13}$$

where the local Reynolds number is given by $Re_x = u_e x/\nu_f$.

3. Stability Analysis

Based on the results obtained, Equations (7)–(9) allow the appearance of the dual solutions. Therefore, by applying the discovery from Merkin [31] and Weidman et al. [32] about the stability of the solutions, long-term stability and dependability of the solution can be determined. To do this, the case of unsteady flow of the boundary value problem Equations (2) and (3) is considered and a new dimensionless time variable τ, is introduced.

$$\frac{\partial u}{\partial t} + u\frac{\partial u}{\partial x} + v\frac{\partial u}{\partial y} = u_e \frac{du_e}{dx} + \frac{\mu_{thnf}}{\rho_{thnf}} \frac{\partial^2 u}{\partial y^2}, \tag{14}$$

$$\frac{\partial T}{\partial t} + u\frac{\partial T}{\partial x} + v\frac{\partial T}{\partial y} = \frac{k_{thnf}}{(\rho C_p)_{thnf}} \frac{\partial^2 T}{\partial y^2}. \tag{15}$$

Then, a new set of dimensionless variables is introduced as follows:

$$\psi = (a\nu_f)^{1/2} xf(\eta, \tau), \theta(\eta, \tau) = \frac{T - T_\infty}{T_w - T_\infty}, \eta = (a\nu_f)^{1/2} y, \ \tau = at. \tag{16}$$

Substituting (16) into Equations (14) and (15), the converted differential equations are attained.

$$\frac{\mu_{thnf}/\mu_f}{\rho_{thnf}/\rho_f} \frac{\partial^3 f}{\partial \eta^3} + f\frac{\partial^2 f}{\partial \eta^2} + 1 - \left(\frac{\partial f}{\partial \eta}\right)^2 - \frac{\partial^2 f}{\partial \eta \partial \tau} = 0, \tag{17}$$

$$\frac{1}{Pr} \frac{k_{thnf}/k_f}{(\rho C_p)_{thnf}/(\rho C_p)_f} \frac{\partial^2 \theta}{\partial \eta^2} + f\frac{\partial \theta}{\partial \eta} - \frac{\partial \theta}{\partial \tau} = 0. \tag{18}$$

While the boundary conditions can be written as follows:

$$f(0,\tau)=0,\frac{\partial f}{\partial \eta}(0,\tau)=\lambda,\theta(0,\tau)=1,\\ \frac{\partial f}{\partial \eta}(\eta,\tau)\to 1,\theta(\eta,\tau)\to 0 \text{ as } \eta\to\infty. \tag{19}$$

Next, the exponential perturbation functions are introduced to as follows [32]:

$$f(\eta,\tau)=f_0(\eta)+e^{-\varepsilon\tau}F(\eta),\\ \theta(\eta,\tau)=\theta_0(\eta)+e^{-\varepsilon\tau}G(\eta), \tag{20}$$

with steady flow solution of $f=f_0(\eta)$ and $\theta=\theta_0(\eta)$ while $F(\eta)$ as well as $G(\eta)$ are relatively small in comparison with $f_0(\eta)$ and $\theta_0(\eta)$ while ε is the unknown eigenvalue. Substituting Equation (20) into Equations (17)–(19) gives:

$$\frac{\mu_{thnf}/\mu_f}{\rho_{thnf}/\rho_f}F'''+f_0F''+f_0F-2f_0'F'+\varepsilon F'=0, \tag{21}$$

$$\frac{1}{Pr}\frac{k_{thnf}/k_f}{(\rho C_p)_{thnf}/(\rho C_p)_f}G''+f_0G'+\theta_0'F+\varepsilon G=0, \tag{22}$$

subject to the boundary conditions:

$$F(0)=0,F'(0)=0,G(0)=0,\\ F'(\eta)\to 0,G(\eta)\to 0 \text{ as } \eta\to\infty. \tag{23}$$

According to Khashi'ie et al. [33], there is no eigenvalues ε can be generated from homogenous boundary conditions. As we can see, Equation (23) is a set of homogenous boundary conditions. Hence, to overcome this problem, nonhomogenous boundary must be considered as a way of attaining the eigenvalues ε. As suggested by Harris et al. [34], the boundary condition $F'(\eta)\to 0$ is relaxed and replaced by $F''(0)=1$, without loss of generalization. The new set of boundary conditions to be considered in this problem is as follows:

$$F(0)=0,F'(0)=0,F''=1,G(0)=0,\\ G(\eta)\to 0 \text{ as } \eta\to\infty. \tag{24}$$

In the meantime, when the eigenvalue problems (21) and (22) subjected to boundary conditions in Equation (24) are solved, an infinite series of eigenvalues $\varepsilon_1<\varepsilon_2<\varepsilon_3\ldots$ can be obtained. The stability of a solution's flow is determined by the positivity of the smallest eigenvalue ε, indicating an initial decay of perturbation. Conversely, if ε is negative, signifying an initial growth of perturbation, the flow is considered unstable.

4. Results and Discussion

The solutions to the mathematical model, as outlined in Equations (7) and (8), subject to the specified boundary conditions in Equation (9), were accomplished by employing a bvp4c solver in the MATLAB software, and the details are explained in Shampine et al. [35]. This solver occupies a finite difference method that employs the three-stage Lobatto IIIa formula with 4-th order accuracy. Beside generating the values of physical quantities for fixed values of parameters, this solver can do the reverse, where it can be used to find the values of the parameters by fixing the values of physical quantities of interest.

We explored the impact of the stretching/shrinking parameter and volume fraction on skin friction, heat transfer, velocity, and temperature profiles. The values were selected through a combination of referencing existing literature and trial-and-error approaches due to the presence of dual solutions. As indicated in Table 2, a Prandtl number value of 6.2 was employed, representing water as the base fluid at a temperature of 25°C following Oztop and Abu-Nada [36]. Therefore, in this study, the parameter Pr is held constant at 6.2, while the parameters φ are systematically adjusted within the range of 0.01–0.05, and the parameters λ are modified within the range of −1.2465 to 2.

The ternary hybrid nanofluid flow, which contains alumina, copper, and titania in water, is considered. The volume fractions of alumina, copper, and titania used in this study are 0.01, 0.03, and 0.05, respectively. The volume fraction of each nanoparticle is evenly distributed at 1/3 to form the ternary hybrid nanofluid, as per the experiment carried out by Ramadhan et al. [22]. Investigating non-unique solutions to the equations governing the current problem is another focus of this work. Additionally, comparison results between the hybrid nanofluid and the ternary hybrid nanofluid are conducted. To ascertain the veracity of the present study results for various values of λ when $\varphi_1=\varphi_2=\varphi_3=0$ are compared with the previous studies, as depicted in Table 3.

The values of $Re_x^{1/2}C_f$ toward λ when $\varphi_1=\varphi_2=\varphi_3=0.01, 0.03$ and 0.05 are depicted in Figure 2. Here is an apparent trend of increasing skin friction values as the volume fractions of nanoparticles increase within a specified range of $-0.65<\lambda<1$. The viscosity of a fluid tends to increase as the volume fractions of solid nanoparticles inside it increase. An elevated viscosity leads to a rise in flow resistance and an increase in skin friction at the interface between the fluid and the surface. Besides, it also can be seen from Figure 2, the skin friction decreases when $\lambda>1$ and no skin friction when $\lambda=1$. Figure 2 also demonstrates the presence of non-unique solutions for the shrinking sheet case in ternary hybrid nanofluid is ranging between $-1.2465<\lambda<-0.9$, where $\lambda_c=-1.2465$ serves as the critical value distinguishing the first and second solutions. Simultaneously, this problem attains a unique solution when $\lambda>-1.2465$. Figure 3 illustrates the observed trend of the Nusselt number exhibiting an increase when the volume fractions are progressively elevated. The Nusselt number is employed to characterize the convective heat transport of a fluid. The

Table 3: $f''(0)$ at various λ when $\varphi_1 = \varphi_2 = \varphi_3 = 0$.

λ	Wang [8]	Bachok et al. [37]	Waini et al. [27]	Present results
2	−1.88731	−1.887307	−1.887307	−1.887307
1.5	*	*	*	−0.873941
1	0	0	0	0
0.5	0.71330	0.713295	0.713295	0.713295
0.25	*	*	*	1.000054
0	1.232588	1.232588	1.232588	1.232588
−0.25	*	*	*	1.402241
−0.5	1.49567	1.49567	1.49567	1.495670
−1	1.32882	1.328817	1.328817	1.328817 [0.00000]
−1.15	1.08223 [0.116702]	1.082231 [0.116702]	1.082231 [0.116702]	1.082231 [0.116702]
−1.2	*	0.932473 [0.233650]	0.932473 [0.233650]	0.9324730 [0.233645]
−1.2465	0.55430	0.584281 [0.554297]	0.584281 [0.554296]	0.5842810 [0.554296]

Note. * Not reported. [ ] Second solution.

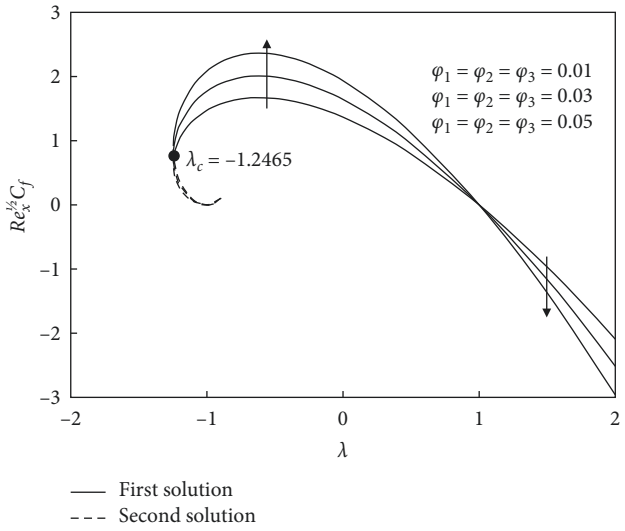

Figure 2: Variations of skin friction coefficient for distinct φ.

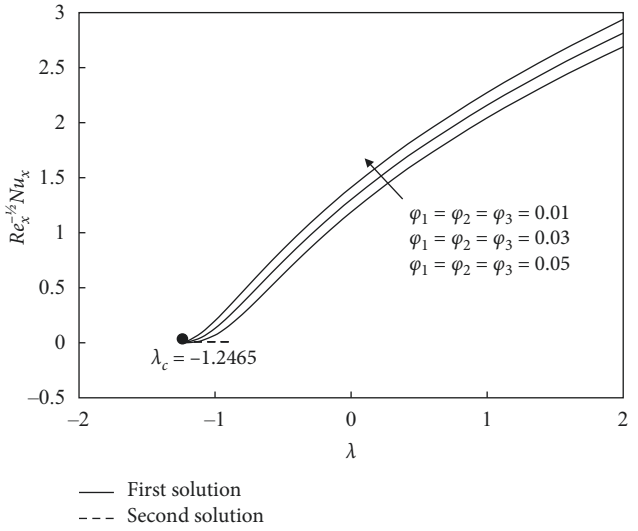

Figure 3: Variations of local Nusselt number for different φ.

escalating volume fractions observed in the stretching/shrinking sheet scenario led to the increased presence of nanoparticles within the same fluid volume, which can enhance the fluid's heat conduction properties due to more particles being available to carry heat energy. Therefore, this phenomenon can potentially increase the rate of heat transfer or the Nusselt number of the fluid.

Figure 4 depicts the velocity profile that elucidates the thinning momentum boundary layer as φ_1, φ_2, and φ_3 increase. Thus, the ternary hybrid nanofluid's velocity gradients increase. This result correlates with the growing pattern of the skin friction coefficient (Figure 2), as it is known that an upsurge in fluid velocity corresponds to the increased surface shear stress. The temperature profile of ternary hybrid nanofluid when φ_1, φ_2, and φ_3 vary from 0.01 to 0.05 is depicted in Figure 5. Physically, it is evident that as φ_1, φ_2 and φ_3 increase, the temperature gradient of the ternary hybrid nanofluid increases, leading to an enhancement in the fluid's convective properties. This outcome is consistent with the conclusion depicted in Figure 3, where an augmentation in convective characteristics leads to an upward trend in the rate of heat transfer in the fluid.

The skin friction and the Nusselt number with respect to a hybrid nanofluid ($\varphi_1 = \varphi_2 = 0.05$) and ternary hybrid nanofluid ($\varphi_1 = \varphi_2 = \varphi_3 = 0.05$) past a shrinking/stretching sheet with the critical point, $\lambda_c = -1.2465$ are shown in Figures 6 and 7, respectively. We can see that both nanofluids possess same critical point, suggesting that certain parameters or conditions are influencing the behavior of both types of nanofluids in a similar manner. The incorporation of φ_3 indicates the development of a ternary hybrid nanofluid, Al_2O_3–Cu–TiO_2/water, derived from the hybrid Al_2O_3–Cu/water nanofluid. This addition boosts the $Re_x^{1/2} C_f$

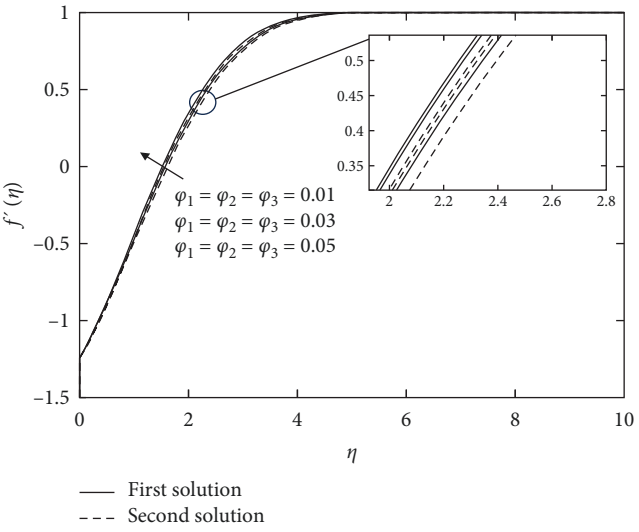

FIGURE 4: φ effect on the velocity profile.

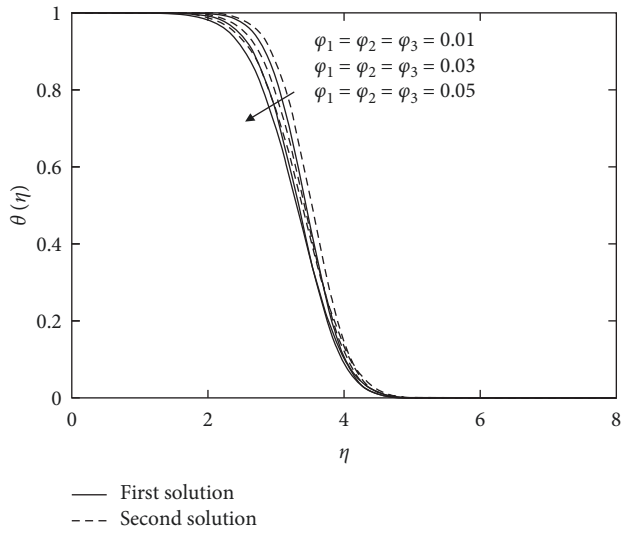

FIGURE 5: φ effect on the temperature profile.

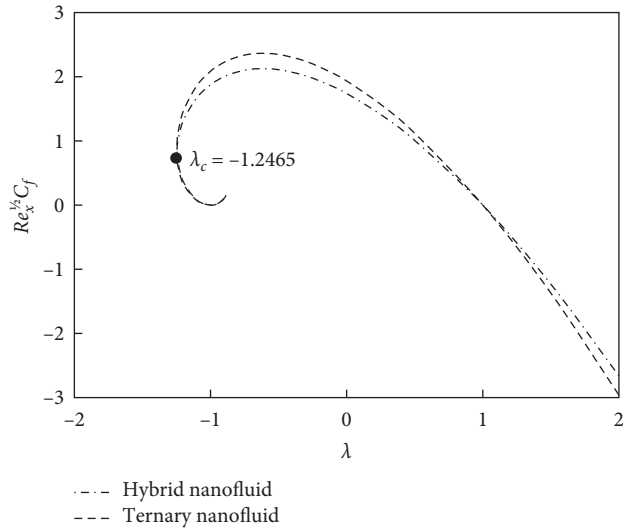

FIGURE 6: Variants of skin friction coefficient with respect to ternary hybrid nanofluid and hybrid nanofluid against λ.

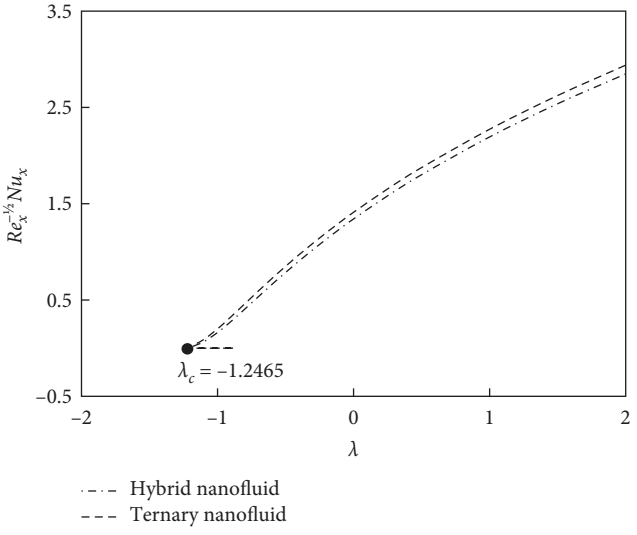

FIGURE 7: Variants of local nusselt number with respect to ternary hybrid nanofluid and hybrid nanofluid against λ.

values when the sheet begins to shrink, as depicted in Figure 6. The reduction in sheet size leads to a diminished surface area, causing an elevation in surface shear stress. While, when φ_3 is introduced, the ternary Al_2O_3–Cu–TiO_2/water hybrid nanofluid become denser in comparison to hybrid Al_2O_3–Cu/water nanofluid, which finally causes the ternary hybrid nanofluid flow velocity to reduce, as depicted in Figure 8.

In Figure 7, trend of the heat transfer rate, $Re_x^{-1/2}Nu_x$ showing an increasing pattern. This outcome validates the hypothesis that, when φ_3 is added, the nanoparticle density can be optimized to enhance the nanofluid heat transfer rate. Hence, ternary hybrid nanofluids evidently demonstrate a superior thermal conductivity rate in comparison to the hybrid nanofluids. Figure 9 depicts the temperature profile, which illustrates the variations in temperature as the hybrid Al_2O_3–Cu/water nanofluid transforms into the ternary hybrid Al_2O_3–Cu–TiO_2/water nanofluid. As the temperature increases, ternary hybrid nanofluid thermal conductivity rises, which may be due to the increase energy conveyed by the rise in nanoparticle fraction of volume over the state of shrinking/stretching sheets. Additionally, it is evident from Figures 4, 5, 8 and 9 that the far-field boundary criteria in Equation (9) were met asymptotically. As emphasized by Ishak [38] it is imperative that velocity and temperature profiles adhere to the specified boundary conditions. This ensures the validation of numerical results as accurate and reliable.

Lastly, the variations of eigenvalue against shrinking/stretching parameter for the ternary hybrid nanofluid ($\varphi_1 = \varphi_2 = \varphi_3 = 0.05$) are presented in Figure 10. From the figure, the sign of smallest eigenvalue ε for the first solution is positive, signifies the stability characteristics of the solutions. Meanwhile, the values of smallest eigenvalue ε for the second

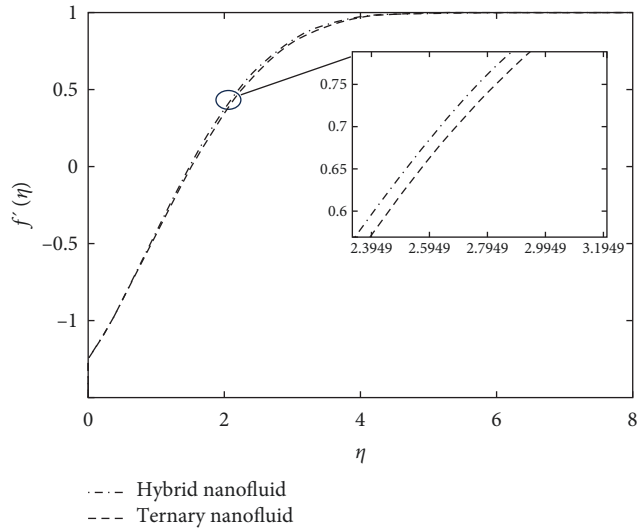

FIGURE 8: Velocity profiles when $\lambda = -1.2465$.

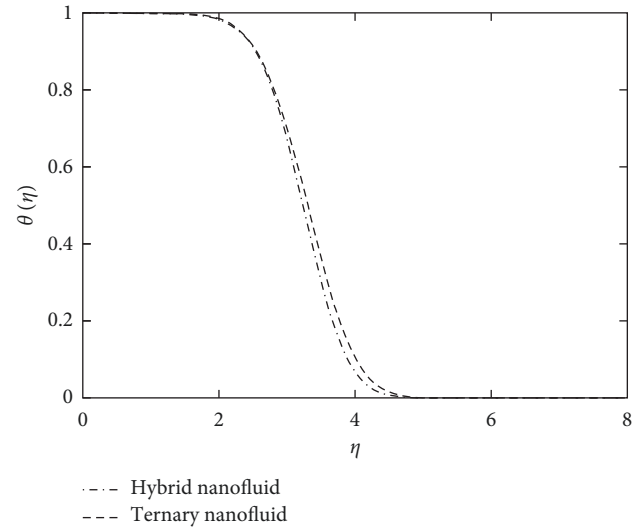

FIGURE 9: Temperature profiles when $\lambda = -1.2465$.

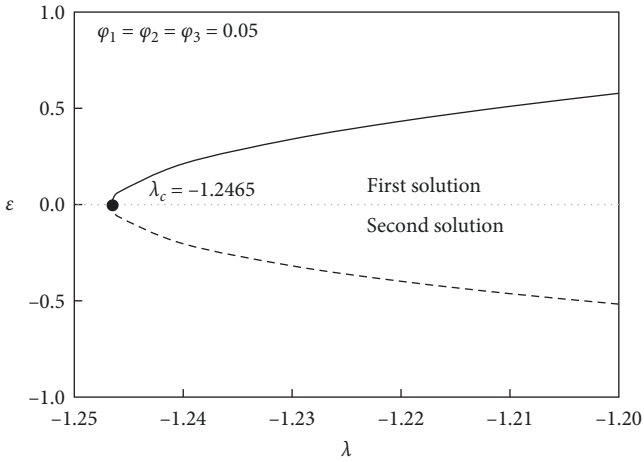

FIGURE 10: Variation of ε against λ.

solution ia negative, indicates the second solution long-term instability.

5. Conclusion

The work on the Hiemenz flow with respect to ternary hybrid nanofluid flow over a stretching/shrinking sheet was concluded. The following insights have been attained:

(i) Within a specific range of shrinking intensity which is $-1.2465 < \lambda < -0.90$, the dual solutions exist while a unique solution exists for $\lambda > -0.90$. The separation between first and second solutions happened at $\lambda_c = -1.2465$ for all volume fraction values considered.

(ii) The stability analysis verified the long-term stability of the first solution, while the second solution was identified as unstable.

(iii) As the nanoparticle volume fraction of ternary hybrid nanofluid Al_2O_3–Cu–TiO_2/water increases, the heat transmission rate rises substantially.

(iv) Based on the findings in comparative analysis, it can be inferred that ternary hybrid nanofluids possess an enhanced heat transfer rate compared to hybrid nanofluids.

Data Availability

The datasets used and/or analyzed during the current study are available from the corresponding author upon reasonable request.

Conflicts of Interest

The authors declare that they have no conflicts of interest.

Authors' Contributions

All authors have equally contributed in the present manuscript.

Acknowledgments

This work has been funded by the Universiti Kebangsaan Malaysia project number "DIP-2023-005". The authors extend their appreciation to the Researchers Supporting Project number (RSPD2024R999), King Saud University, Riyadh, Saudi Arabia.

References

[1] E. G. Fisher, *Extrusion of Plastics*, John Wiley & Sons, 1976.

[2] Y. Zheng, N. A. Ahmed, and W. Zhang, "Heat dissipation using minimum counter flow jet ejection during spacecraft re-entry," *Procedia Engineering*, vol. 49, pp. 271–279, 2012.

[3] K. Affeld, A. J. Reininger, J. Gadischke, K. Grunert, S. Schmidt, and F. Thiele, "Fluid mechanics of the stagnation point flow chamber and its platelet deposition," *Artificial Organs*, vol. 19, no. 7, pp. 597–602, 1995.

[4] T. Yamaguchi, A. A. Basri, K. A. Bin Ahmad, and M. Tamagawa, "Prediction of thrombus formation on

impinging jet flow by eulerian computational fluid dynamics (CFD) effects of concentration boundary conditions on platelet adhesion," *International Journal of Innovative Computing, Information and Control*, vol. 18, no. 2, pp. 657–666, 2022.

[5] K. Hiemenz, "Die Grenzschicht an einem in den gleichformigen Flussigkeitsstrom eingetauchten geraden Kreiszylinder," *Dingler's Polytechnical Journal*, vol. 326, pp. 321–324, 1911.

[6] F. Homann, "Der einfluß großer zähigkeit bei der strömung um den zylinder und um die kugel," *ZAMM-Journal of Applied Mathematics and Mechanics*, vol. 16, no. 3, pp. 153–164, 1936.

[7] T. R. Mahapatra and A. S. Gupta, "Stagnation-point flow towards a stretching surface," *The Canadian Journal of Chemical Engineering*, vol. 81, no. 2, pp. 258–263, 2003.

[8] C. Y. Wang, "Stagnation flow towards a shrinking sheet," *International Journal of Non-Linear Mechanics*, vol. 43, no. 5, pp. 377–382, 2008.

[9] M. R. Turner and P. Weidman, "Homann stagnation-point flow impinging on a biaxially stretching surface," *European Journal of Mechanics-B/Fluids*, vol. 86, pp. 49–56, 2021.

[10] G. M. Sarkar and B. Sahoo, "On dual solutions of the three-dimensional Hiemenz flow over a stretching/shrinking sheet," *ZAMM-Journal of Applied Mathematics and Mechanics*, vol. 102, no. 9, Article ID e202100043, 2022.

[11] I. Mustafa, Z. Abbas, A. Arif, T. Javed, and A. Ghaffari, "Stability analysis for multiple solutions of boundary layer flow towards a shrinking sheet: analytical solution by using least square method," *Physica A: Statistical Mechanics and its Applications*, vol. 540, Article ID 123028, 2020.

[12] A. Jamaludin, R. Nazar, and I. Pop, "Mixed convection stagnation-point flow of cross fluid over a shrinking sheet with suction and thermal radiation," *Physica A: Statistical Mechanics and its Applications*, vol. 585, Article ID 126398, 2022.

[13] S. U. S. Choi and J. A. Eastman, "Enhancing thermal conductivity of fluids with nanoparticles," in *Proceedings of the 1995 ASME International Mechanical Engineering Congress and Exposition*, pp. 99–105, USDOE, Washington, DC, 1995.

[14] R. Mohebbi and M. M. Rashidi, "Numerical simulation of natural convection heat transfer of a nanofluid in an L-shaped enclosure with a heating obstacle," *Journal of the Taiwan Institute of Chemical Engineers*, vol. 72, pp. 70–84, 2017.

[15] A. Gavili and T. Isfahani, "Experimental investigation of transient heat transfer coefficient in natural convection with Al_2O_3-nanofluids," *Heat and Mass Transfer*, vol. 56, no. 3, pp. 901–911, 2020.

[16] M. Turkyilmazoglu, "Single phase nanofluids in fluid mechanics and their hydrodynamic linear stability analysis," *Computer Methods and Programs in Biomedicine*, vol. 187, Article ID 105171, 2020.

[17] A. A. A. Arani and H. Aberoumand, "Stagnation-point flow of Ag-CuO/water hybrid nanofluids over a permeable stretching/shrinking sheet with temporal stability analysis," *Powder Technology*, vol. 380, pp. 152–163, 2021.

[18] N. S. Khashi'ie, I. Waini, I. Pop, N. A. Zainal, and A. R. M. Kasim, "Axisymmetric hybrid nanofluid flow due to a convectively heated stretching/shrinking disk," *Journal of Advanced Research in Fluid Mechanics and Thermal Sciences*, vol. 85, no. 1, pp. 113–124, 2021.

[19] I. Waini, A. Ishak, and I. Pop, "Unsteady flow and heat transfer past a stretching/shrinking sheet in a hybrid nanofluid," *International Journal of Heat and Mass Transfer*, vol. 136, pp. 288–297, 2019.

[20] I. Pop, T. Groşan, C. Revnic, and A. V. Roşca, "Unsteady flow and heat transfer of nanofluids, hybrid nanofluids, micropolar fluids and porous media: a review," *Thermal Science and Engineering Progress*, vol. 46, Article ID 102248, 2023.

[21] M. V. Bndu and G. M. J. Herbert, "Thermal conductivity and viscosity of Al_2O_3–ZnO–MWCNT-EG ternary nanofluid," *International Journal of Energy Research*, vol. 46, no. 12, pp. 17478–17496, 2022.

[22] A. I. Ramadhan, W. H. Azmi, and R. Mamat, "Experimental investigation of thermo-physical properties of tri-hybrid nanoparticles in water-ethylene glycol mixture," *Walailak Journal of Science and Technology (WJST)*, vol. 18, no. 8, Article ID 9335, 2021.

[23] L. S. Sundar, K. V. V. C. Mouli, Z. Said, and A. C. M. Sousa, "Heat transfer and second law analysis of ethylene glycol-based ternary hybrid nanofluid under laminar flow," *Journal of Thermal Science and Engineering Applications*, vol. 13, no. 5, 2021.

[24] I. L. Animasaun, S.-J. Yook, T. Muhammad, and A. Mathew, "Dynamics of ternary-hybrid nanofluid subject to magnetic flux density and heat source or sink on a convectively heated surface," *Surfaces and Interfaces*, vol. 28, Article ID 101654, 2022.

[25] G. Gupta and P. Rana, "Comparative study on Rosseland's heat flux on three-dimensional MHD stagnation-point multiple slip flow of ternary hybrid nanofluid over a stretchable rotating disk," *Mathematics*, vol. 10, no. 18, Article ID 3342, 2022.

[26] Z. Xuan, Y. Zhai, M. Ma, Y. Li, and H. Wang, "Thermo-economic performance and sensitivity analysis of ternary hybrid nanofluids," *Journal of Molecular Liquids*, vol. 323, Article ID 114889, 2021.

[27] I. Waini, A. Ishak, and I. Pop, "Hiemenz flow over a shrinking sheet in a hybrid nanofluid," *Results in Physics*, vol. 19, Article ID 103351, 2020.

[28] S. P. A. Devi and S. S. U. Devi, "Numerical investigation of hydromagnetic hybrid Cu–Al_2O_3/water nanofluid flow over a permeable stretching sheet with suction," *International Journal of Nonlinear Sciences and Numerical Simulation*, vol. 17, no. 5, pp. 249–257, 2016.

[29] Z. Mahmood, N. A. Ahammad, S. E. Alhazmi, U. Khan, and M. Z. Bani-Fwaz, "Ternary hybrid nanofluid near a stretching/shrinking sheet with heat generation/absorption and velocity slip on unsteady stagnation point flow," *International Journal of Modern Physics B*, vol. 36, no. 29, Article ID 222502095, 2022.

[30] F. M. White and J. Majdalani, *Viscous Fluid Flow*, Vol. 3, McGraw-Hill, New York, 2006.

[31] J. H. Merkin, "A model for isothermal homogeneous-heterogeneous reactions in boundary-layer flow," *Mathematical and Computer Modelling*, vol. 24, no. 8, pp. 125–136, 1996.

[32] P. D. Weidman, D. G. Kubitschek, and A. M. J. Davis, "The effect of transpiration on self-similar boundary layer flow over moving surfaces," *International Journal of Engineering Science*, vol. 44, no. 11-12, pp. 730–737, 2006.

[33] N. S. Khashi'ie, N. M. Arifin, I. Pop, R. Nazar, and E. H. Hafidzuddin, "A new similarity solution with stability analysis for the three-dimensional boundary layer of hybrid nanofluids," *International Journal of Numerical Methods for Heat & Fluid Flow*, vol. 31, no. 3, pp. 809–828, 2020.

[34] S. D. Harris, D. B. Ingham, and I. Pop, "Mixed convection boundary-layer flow near the stagnation point on a vertical surface in a porous medium: brinkman model with slip," *Transport in Porous Media*, vol. 77, no. 2, pp. 267–285, 2009.

[35] L. F. Shampine, I. Gladwell, and S. Thompson, *Solving ODEs with MATLAB*, Cambridge University Press, 1st edition, 2003.
[36] H. F. Oztop and E. Abu-Nada, "Numerical study of natural convection in partially heated rectangular enclosures filled with nanofluids," *International Journal of Heat and Fluid Flow*, vol. 29, no. 5, pp. 1326–1336, 2008.
[37] N. Bachok, A. Ishak, and I. Pop, "Boundary layer stagnation-point flow toward a stretching/shrinking sheet in a nanofluid," *Journal of Heat Transfer*, vol. 135, no. 5, Article ID 054501, 2013.
[38] A. Ishak, "Aliran lapisan sempadan bersebelahan plat tegak dengan suhu permukaan malar (boundary layer flow adjacent to a vertical plate with constant surface temperature)," *Sains Malaysiana*, vol. 39, no. 6, pp. 1035–1039, 2010.